The error in the phases increases slightly if the error in the data increases from $\sigma = 0{\cdot}00$ to $\sigma = 0{\cdot}04$ whereas from $\sigma = 0{\cdot}04$ to $\sigma = 0{\cdot}08$ the increase in phase error is much stronger. In reality, however, the standard deviation of the (random) error will be smaller than 0·08, but the data will be affected by systematic errors as well.

The results reported in the present paper show that it is possible to estimate triplet invariants from artificial two-wavelength data (which may be corrupted by random errors) and use the invariants in a multi-solution procedure to obtain structure-factor phases without the need to solve the heavy-atom structure.

References

FORTIER, S., WEEKS, C. M. & HAUPTMAN, H. (1984). *Acta Cryst.* **A40**, 544-548.
GIACOVAZZO, C. (1983). *Acta Cryst.* **A39**, 585-592.
HAUPTMAN, H. (1982*a*). *Acta Cryst.* **A38**, 289-294.
HAUPTMAN, H. (1982*b*). *Acta Cryst.* **A38**, 632-641.
HENDRICKSON, W. A. (1973). *Biophysical Applications of Crystallography Techniques*, pp. 61-83. *Trans. Am. Crystallogr. Assoc.*
HULL, E. & IRWIN, M. J. (1978). *Acta Cryst.* **A34**, 863-870.
KARLE, J. (1984). *Acta Cryst.* **A40**, 526-531.
KARLE, J. (1989). *Acta Cryst.* **A45**, 303-307.
KLOP, E. A., KRABBENDAM, H. & KROON, J. (1989*a*). *Acta Cryst.* **A45**, 203-208.
KLOP, E. A., KRABBENDAM, H. & KROON, J. (1989*b*). *Acta Cryst.* **A45**, 609-613.
KROON, J., SPEK, A. L. & KRABBENDAM, H. (1977). *Acta Cryst.* **A33**, 382-385.
MAIN, P., FISKE, S. J., HULL, S. E., LESSINGER, L., GERMAIN, G., DECLERQ, J.-P. & WOOLFSON, M. M. (1980). *MULTAN80. A System of Computer Programs for the Automatic Solution of Crystal Structures from X-ray Diffraction Data.* Univs. of York, England, and Louvain, Belgium.
PITTS, J. E., TICKLE, I. J., WOOD, S. P. & BLUNDELL, T. L. (1982). *Sov. Phys. Crystallogr.* **27**(1), 56-62.
SIEKER, L. C., ADMAN, E. T. & JENSEN, L. H. (1972). *Nature (London)*, **235**, 40-42.
WOOLFSON, M. M. & YAO JIA-XING (1988). *Acta Cryst.* **A44**, 410-413.

Acta Cryst. (1990). **A46**, 526-534

X-ray Transmissivity Measurements using Dynamical Diffraction under Grazing-Incidence Conditions

BY F. RIEUTORD

Institut Laue-Langevin, BP 156*X*, 38042 *Grenoble CEDEX, France*

(*Received* 12 *October* 1989; *accepted* 5 *February* 1990)

Abstract

The dependence of the X-ray transmission coefficient of a thin-film coating as a function of incidence has been measured in the grazing-angle range. The method is based on the use of a substrate Bragg reflection to redirect the incident or transmitted beams. It allows grazing incidence from both outside and inside the substrate to be performed. The geometry of the experiment is described. The results are interpreted by means of dynamical theory combined with an optical formalism for stratified systems. Experimental results and applications are compared with reflectivity data.

1. Introduction

Surface and thin-film studies using X-ray or neutrons in glancing-incidence geometries have undergone considerable development in recent years. In these studies, one makes use of the different signals from a sample when struck by a grazing beam such as, for instance, specular reflection in the reflectivity technique (Parratt, 1954), diffracted beams in grazing-incidence scattering (GIS) (Marra, Eisenberger & Cho, 1979) or even fluorescence (Brunel, 1986). Glancing angles are used in these techniques to limit the penetration depth and thus to enhance the sensitivity to the near-surface volume. Therefore, bulk substrate scattering is often considered as a nuisance in these experiments. The aim of this paper is to show that it is possible to take advantage of the substrate to perform measurements of the transmission coefficient which can provide useful information, complementing data from other techniques.

The interpretation of the data of grazing-incidence techniques is often made by means of kinematical theory (Born approximation). Such an approximation is justified by the weak coupling between X-rays (or neutrons) and matter. When the incidence angle is close to the critical angle for total reflection, this approximation has to be removed since multiple-scattering effects become important. Improvement of simple Born approximations can be made [*e.g.* distorted-wave Born approximation (Vineyard, 1982)] but the most general way of performing the calculations

0108-7673/90/060526-09$03.00 © 1990 International Union of Crystallography

is to use dynamical theory. This theory is very general and includes all the effects of surface scattering (Durbin & Gog, 1989) but is well suited for semi-infinite single crystals only. We shall show here how we can use this theory to interpret experimental results when the crystal surface is coated with a thin film and especially how we can couple this theory to the optical formalism for stratified media used for instance in reflectivity calculations. The experimental part of the work concentrates on the investigation of a multilayer adsorbate deposited over a silicon substrate.

2. Geometrical description of the method

For most thin films, measurements in the transmission mode are impossible due to the presence of the substrate which is opaque to the radiation, especially when the incidence angle is small since the travelling length through the substrate is large. For this reason, there have been no transmission measurements as a function of incidence, to our knowledge, so far.

A straightforward way of solving this problem would be to use free-standing films or very thin substrates (Rieutord, Benattar & Bosio, 1986) but grazing-incidence experiments require large flat areas which are incompatible with this kind of preparation. Moreover, in many techniques, substrates do play an important role in the building of the films and cannot be removed.

In our case, we take advantage of the substrate. The basic idea is to use the substrate as a mirror to reflect the transmitted beam out of the sample. The simplest way would be to use specular reflection at the film/substrate interface. Such a reflection has already been used for instance for generating a standing-wave pattern allowing investigation of the deposited film (Bedzyk, Bommarito & Schildkraut, 1989; Authier, Gronkowski & Malgrange, 1989). It is not suitable however for our purpose since its amplitude is of the same order of magnitude as the reflections from other density gradients in the film and its effect is merely a contribution to the overall reflectivity of the system.

Thus, as for the classical standing-wave technique, we have used the reflection from the Bragg planes of the substrate (Fig. 1). The advantage of this technique is that reflection remains high even at large angles of incidence. The main problem is that this reflection occurs only for a definite orientation (the so-called Bragg angle θ_B) of the Bragg planes with respect to the incidence beam, whereas we need to vary the incidence of the beam with respect to the surface (denoted by i from now on).

Previous studies (Brümmer, Höche & Nieber, 1976; Kishino, Noda & Kohra, 1972) aimed at a measure of the intensity of a Bragg reflection as a function of i (so-called asymmetric Bragg-case diffraction) just used different samples with surfaces cut along different orientations with respect to the Bragg planes, according to the relation

$$i + \alpha - \theta_B = 0, \tag{1}$$

where α is the angle between the normal to the Bragg planes $\mathbf{n}_B$ and the normal to the surface $\mathbf{n}_S$. Obviously such a method cannot be applied in our case since we want to study the same deposit for a continuous range of incident angles.

The solution we have derived for this problem is to use a reflection on Bragg planes whose normals do not lie in the plane of incidence π_S (defined by the directions of the incident beam $\mathbf{u}_i$ and the normal $\mathbf{n}_S$ to the surface), *i.e.* use a geometry where the incidence plane for surface reflection (π_S) is distinct from the incidence plane for Bragg reflection (π_B). Relation (1) is then replaced by a relation involving a supplementary degree of freedom which is the orientation of these two planes with respect to each other or equivalently the rotation angle φ of $\mathbf{n}_B$ about $\mathbf{n}_S$ (Fig. 2). This relation reads

$$\cos \varphi = \frac{\sin \theta_B - \sin i \cos \alpha}{\cos i \sin \alpha}, \tag{2}$$

obtained from angular relations in the spherical triangle ($\mathbf{u}_i, \mathbf{n}_B, \mathbf{n}_S$).

Varying φ will enable us to vary the incidence while maintaining the Bragg condition on a set of reticular

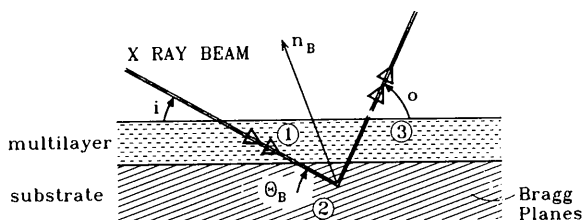

Fig. 1. Schematic view illustrating the principle of the method. The X-ray beam crosses the film at the entrance, is reflected by the atomic planes of substrate and crosses the film once again at the exit. Note that the incident and diffracted rays are not actually in the same plane.

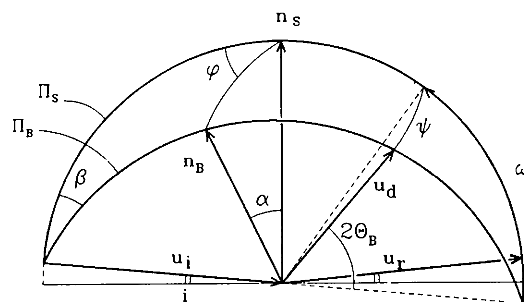

Fig. 2. Geometry of the experiment. $\mathbf{u}_i$, $\mathbf{u}_d$ and $\mathbf{u}_r$ are the directions of the incident, Bragg-reflected and surface-reflected waves. $\mathbf{n}_S$ and $\mathbf{n}_B$ are the normals to surface and Bragg planes, respectively.

planes of the substrate. To record the diffracted beam, the detector will have to be moved out of the π_S plane as well. The two angles ψ and ω defining the position of the detector (see Fig. 2) are given by

$$\tan \omega = \tan (2\theta_B) \cos \beta,$$

$$\tan \psi = \sin (2\theta_B) \sin \beta,$$

where

$$\cos \beta = \frac{\cos \alpha - \sin \theta_B \sin i}{\cos \theta_B \cos i}.$$

A schematic view of the four-circle diffractometer used for the experiment with the corresponding angles i, φ, ω, ψ is shown in Fig. 3.

The same geometry has been used in a previous study (Brunel & de Bergevin, 1986) where the intensity and shape of Bragg peaks were investigated as a function of the grazing incidence.

2.1. *Choice of the Bragg reflection*

Relation (2) will have a solution for φ at incidences including grazing angles ($i \simeq 0$) only if the Bragg angle θ_B is smaller than α. We report in Table 1 the list of values of α and θ_B for low-index Bragg reflections [silicon (100) substrate, λCu $K\alpha$].

The condition $\theta_B < \alpha$ reads

$$(h^2+k^2)^{1/2}/(h^2+k^2+l^2) > \lambda/2a, \qquad (3)$$

where $a = 5{\cdot}43$ Å is the side of the cubic cell of silicon and $\lambda = 1{\cdot}54$ Å is the wavelength.

2.2. *Outgoing beam*

Another important aspect of the geometry is that it allows not only grazing incidences for the incident beam but also for the outgoing beam. Denoting the angle of the diffracted beam with respect to the surface by o, we have

$$\sin o = -\sin i + 2 \sin \theta_B \cos \alpha,$$

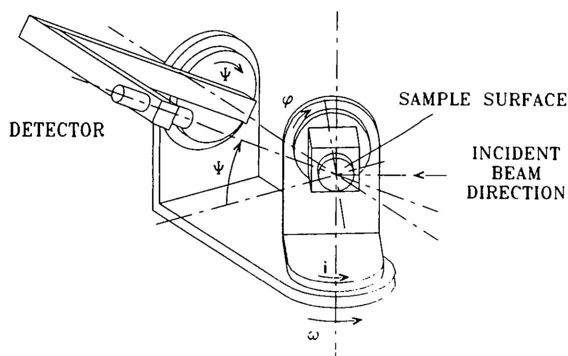

Fig. 3. Schematic view of the four-circle diffractometer used for the experiment. The angular movements i, ω, φ and ψ correspond to the angles shown in Fig. 2.

Table 1. *List of low-index Bragg reflections with the corresponding angles Θ_B, α and i_S; only those satisfying $\Theta_B < \alpha$ can be used for transmission measurements*

$h\ k\ l$	θ_B	α	i_S	Possible use
1 1 1	14·21	54·74	16·48	Yes
2 2 0		45	34·56	Yes
2 0 2	23·65	45	34·56	Yes
0 2 2		90	0	No (vert. planes)
3 1 1		25·24	—	No
1 3 1	28·05	72·45	16·48	Yes
1 1 3		72·45	16·48	Yes
4 0 0		0	—	No
0 4 0	34·56	90	0	No (vert. planes)
0 0 4		90	0	No (vert. planes)
3 3 1		46·51	58·31	Yes
3 1 3	38·19	46·51	58·31	Yes
1 3 3		76·74	16·48	Yes

which shows that, when $\sin i$ comes close to $2 \sin \theta_B \cos \alpha$, o becomes very small (since $\theta_B < \alpha$, $2 \sin \theta_B \cos \alpha < 1$). The angle i_S corresponding to a zero output angle has also been reported in Table 1. The possibility of achieving low output angles is simply a consequence of the symmetry between incident and diffracted beams.

It should be noted that the angle i_S is large for most reflections (*e.g.* $i_S = 34{\cdot}6°$ for the 220 reflection we shall consider later on) so that the grazing condition will not occur simultaneously for incident and diffracted beams. The only exception to this is the case of planes perpendicular or nearly perpendicular to the surface.

This case corresponds to grazing-incidence diffraction geometry (GID). GID has been studied extensively in recent years (Marra, Eisenberger & Cho, 1979; Dosch, Batterman & Wack, 1986; Sakata & Hashizume, 1988) and we shall not consider this particular case here. Note however that the dynamical treatment given below applies to this case as well.

Finally, there is another way of doing a similar experiment (Sauvage, 1989), which would be especially well suited to synchrotron radiation since it would take advantage of the possibility of changing λ. If λ and i are chosen according to

$$\lambda = 2d \sin \alpha \bigg/ \left[1 - \frac{q_S d}{2\pi} \cos \alpha + \frac{q_S^2 d^2}{(2\pi)^2}\right]^{1/2}$$

and $q_S = 4\pi(\sin i)/\lambda$, where q_S is the wave-vector transfer for the surface reflection, the Bragg condition will be satisfied without requiring orientation of the Bragg reflection out of the plane of incidence π_S. Monochromation at the required wavelength could be achieved by the substrate Bragg reflection itself just sending a white beam over the sample under incidence i. Note, however, that changes in wavelength make the modelling (index) somewhat more complicated.

3. Calculation of the diffracted intensity

The path of the X-ray beam in the previous geometry involves two transmissions through the film (at the entrance and at the exit) and a reflection in the substrate. Propagation of electromagnetic waves through these two media can be described using two formalisms derived from Maxwell equations: dynamical theory for the crystalline substrate and transfer-matrix formalism for the film. In this section, we shall examine how they can be coupled together to yield the diffracted intensity as a function of incidence and how the transmission is related to this intensity.

3.1. *Dynamical theory*

The propagation of X-rays in a perfect crystal is given by the solution of Maxwell equations in a three-dimensional periodic medium. Expanding the index of refraction and the different waves in Fourier series and assuming a simple Bragg reflection takes place, one finds that the incident and diffracted wavefields must satisfy the following equations (James, 1982; Batterman & Cole, 1964):

$$\begin{cases}[(K_H^2-k^2)/K_H^2]D_H=\varphi_0 D_H+\varphi_H D_{0[H]}\\ [(K_0^2-k^2)/K_0^2]D_0=\varphi_{\bar{H}} D_{H[0]}+\varphi_0 D_0,\end{cases}\tag{4}$$

where $D_{i[j]}$ is the projection of the electric induction $\mathbf{D}_i$ on the plane normal to $\mathbf{K}_j$. The indices 0 and H stand for incident and diffracted waves, respectively.

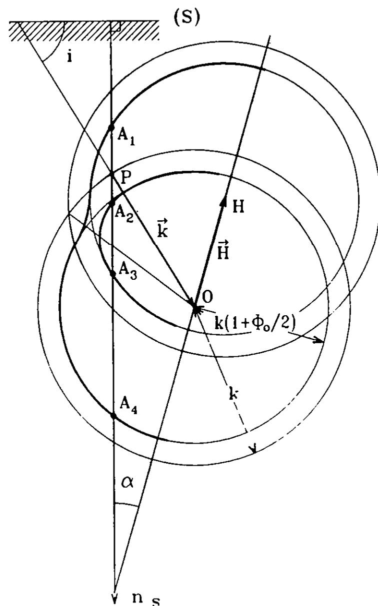

Fig. 4. Dispersion surface. The intersections of this surface with the normal to the sample surface are the four tie points A_i. **H** is the reciprocal-lattice vector of the set of Bragg planes.

φ_i are the Fourier components of the polarizability.

The condition that these equations should have a solution is

$$[(K_H^2-k^2)/K_H^2-\varphi_0][(K_0^2-k^2)/K_0^2-\varphi_0]=P^2\varphi_H\varphi_{\bar{H}},\tag{5}$$

where P is the polarization factor [1 for s, $\cos(2\theta_B)$ for p].

Phase matching at any interface parallel to the surface requires that the tangential components of the internal wave vectors ($\mathbf{K}_i$) equal those of the external wave vectors ($\mathbf{k}_i$).

$$\mathbf{k}_{i\|}=\mathbf{K}_{i\|}.\tag{6}$$

Thus we can set $\mathbf{K}_0=\mathbf{k}_0-gk\mathbf{n}$, and substituting into (5) yields a fourth-order equation in g which reads, using standard notation (*e.g.* Bedynska, 1973, 1974; Hartwig, 1976, 1977; Rustichelli, 1975),

$$g^4+(A+B)g^3+(AB+C+2X_1)g^2+[X_1(A+B)+AC]g+(X_1C+X_2)=0,\tag{7}$$

where, in our geometry,

$$\begin{cases}A=-2\sin i\\ B=4\sin\Theta_B\cos\alpha-2\sin i\\ C=4\sin^2\Theta_B-4\sin\Theta_B\\ \qquad\times(\cos i\sin\alpha\cos\varphi+\sin i\cos\alpha)\\ X_1=-\dfrac{\varphi_0(1-\varphi_0)+p^2\varphi_H\varphi_{\bar{H}}}{(1-\varphi_0)^2-p^2\varphi_H\varphi_{\bar{H}}},\\ X_2=\dfrac{\varphi_0^2-p^2\varphi_H\varphi_{\bar{H}}}{(1-\varphi_0)^2-p^2\varphi_H\varphi_{\bar{H}}}.\end{cases}\tag{8}$$

A graphical solution of (5) and (7) can be obtained by constructing the dispersion surface defined as the loci of the extremities of all vectors $\mathbf{K}_0$ satisfying (5). The pairs ($\mathbf{K}_0, \mathbf{K}_H$) of waves allowed to propagate in the crystal are those satisfying condition (6). The origin of these vectors is at the intersection between the normal to the surface and the dispersion surface (see Fig. 4), the so-called tie points A_n.

Therefore, for each incidence angle there will be in general four pairs of wave vectors ($\mathbf{K}_{0n}, \mathbf{K}_{Hn}$), possibly complex, allowed to propagate in the substrate. For each pair of waves the ratio of incident to diffracted amplitude will be given from (5) by

$$\frac{D_{Hn}}{D_{0n}}=\frac{1}{\varphi_{\bar{H}}}\left(\frac{g_n^2+Ag_n}{1+g_n^2+Ag_n}-\varphi_0\right)=X_n.\tag{9}$$

3.2. *Boundary conditions*

Up to this point, the nature of the surface itself has not been taken into account; the boundary conditions will fix the repartition of the intensity between the

different wavefields and yield the intensity of the beam diffracted out of the crystal.

3.2.1. *General considerations.* Since the substrate used in the experiment is thick, we may consider it as a semi-infinite crystal. Thus, all the waves corresponding to g_i with $\mathrm{Im}\,(g_i)<0$ have to be physically excluded because they would have an amplitude ever increasing with depth. We are then left with two pairs of waves. In the standard case of a crystal surface, boundary conditions are simply equality conditions for parallel and perpendicular components of the electric and magnetic fields, respectively. Here, the relations have to account for the propagation in the film coverage.

3.2.2. *Transfer matrices.* The problem of the propagation of light in stratified media is a classical problem of optics (Abelès, 1950; Born & Wolf, 1984). It has been shown that such a medium may be fully described by a 2×2 unimodular characteristic matrix M. This formalism also holds in the X-ray range and has been widely used in the characterization of multilayer film by X-ray reflectivity.

The characteristic matrix M is actually a transfer matrix which relates the component of the electric and magnetic fields on one side of the film to the components on the other side. Thus, it is well suited to express our boundary conditions which read

$$\begin{pmatrix} D_{01}+D_{02} \\ \Gamma_{01}D_{01}+\Gamma_{02}D_{02} \end{pmatrix} = (M_d^{-1}) \begin{pmatrix} D_0+D_r \\ \Gamma_0(D_0-D_r) \end{pmatrix} \quad (10)$$

for the incident waves and

$$\begin{pmatrix} D_{H1}+D_{H2} \\ \Gamma_{H1}D_{H1}+\Gamma_{H2}D_{H2} \end{pmatrix} = (M_i) \begin{pmatrix} D_H \\ \Gamma_H D_H \end{pmatrix} \quad (11)$$

for the diffracted waves.

In these expressions $\Gamma_\alpha=\mathbf{K}_\alpha\,.\,\mathbf{n}_S/K_\alpha^2$ and D_0, D_r, D_H are the electric inductions of the incident, reflected and diffracted waves.

3.2.3. *Expression for the matrices.* In (10) and (11) the matrices M_d and M_i are transfer matrices for wave propagation in the air→substrate and substrate→air directions. It should be noted that they are not related in any simple way since a matrix depends not only on the index profile of the system but also on an invariant which is $(K_\parallel)$ (*i.e.*, in optics, the invariant $n\cos i$ of Snell's law).

Here $K_{0\parallel}$ and $K_{H\parallel}$ are different since $\mathbf{H}$ has a component in the plane of the surface.

Also, the two index profiles of M_d and M_i are symmetric to each other. If we assume that the profile may be broken into a series of n homogeneous laminae then

$$M_d=\pi_{j=1}^{n}M_j \quad \text{and} \quad M_i=\pi_{j=n}^{1}M_j$$

and except in the case $n=1$ no simple relationship exists between these two matrices, even at a same value of $(K_\parallel)$.

It should also be noted that the expression for the matrices depends on the polarization but this effect is small at glancing angle and we neglect it. At large angle $M\simeq I$ in both cases.

3.2.4. *Derivation of the transmissivity.* The set of equations (9), (10), (11) allows a determination of both D_r/D_0 and D_H/D_0 and consequently of the reflected and diffracted intensities for any value of the incidence angle i:

$$I_R=|D_R/D_0|^2, \qquad I_H=[\mathrm{Re}\,(\Gamma_H)/\mathrm{Re}\,(\Gamma_0)]|D_H/D_0|^2.$$

We shall now discuss how these two quantities are related to standard expressions for reflectivity and transmissivity in the case of grazing incidence.

Reflection and transmission coefficients in the standard configuration (*i.e.* when no diffraction occurs in the substrate) are solutions of

$$(M_d^{-1}) \begin{pmatrix} D_0+D_r \\ \Gamma_0(D_0-D_r) \end{pmatrix} = \begin{pmatrix} D_t \\ \Gamma_t D_t \end{pmatrix} \quad (12)$$

where

$$\Gamma_t=\mathbf{K}_t\,.\,\mathbf{n}/K_t^2.$$

Comparison of (12) and (10) shows that, due to the presence of two waves propagating in slightly different directions, transmission and reflection will differ when the substrate is in Bragg reflection position.

This difference remains small, however, except in the case of $\Theta\sim\Theta_c$ and it cancels exactly at an incidence corresponding to the centre of the Darwin curve (see Fig. 5). In practice, due to the divergence of the incident beam, one averages over a finite width which is comparable to, or larger than, the Darwin width and discrepancies on each side cancel.

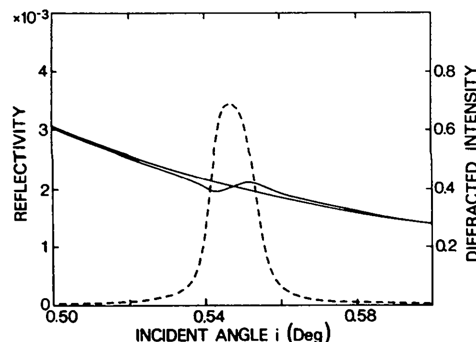

Fig. 5. Reflected and diffracted intensities as a function of incidence for a single-crystal silicon surface. The standard reflectivity has also been drawn to show the influence of Bragg reflection on surface reflection. Note the shift of the Darwin curve ($i_0=0{\cdot}50°$).

The assumption that the reflection coefficient is unchanged means that (10) is equivalent to (12), *i.e.*

$$\begin{pmatrix} D_{01}+D_{02} \\ \Gamma_{01}D_{01}+\Gamma_{02}D_{02} \end{pmatrix} = \begin{pmatrix} D_t \\ \Gamma_t D_t \end{pmatrix}.$$

If one puts $M_i = I$ into (10) according to the large exit angle, this shows that $D_H = \alpha D_t$ where the proportionality coefficient is independent of the matrix M_d, *i.e.* of the coverage. The diffracted intensity $|D_H/D_0|$ is thus proportional to the transmission coefficient t and the proportionality coefficient may be viewed as a reflection coefficient for the substrate. Note that such results are not valid when the incident angle is less than or close to i_c or when both incident and take-off angles are small. In this case, significant changes to the reflection are induced by the Bragg reflection (see *e.g.* Cowan, 1985) and the calculation of the diffracted intensity has to be made using the complete set of equations (9), (10) and (11).

3.2.5. *Shape of the Darwin curve.* Let us consider first the case of a single-crystal surface. At large angles, the width and the shift of the Darwin curve with respect to the geometrical Bragg position increase with decreasing incidences. For small incidences, this shift tends to the critical angle i_c and the width decreases again, due to the truncation of the Darwin curve at $i = i_c$. Correspondingly, the value of φ for a maximum intensity at $i = i_0$ is shifted from its geometrical position given by (2).

The total diffracted intensity is obtained by integration of the Darwin curve. Experimentally, the divergence of the incident beam (0·1 mrad) is often greater than the Darwin width. Special attention has to be paid to the low incidence case where these widths are similar.

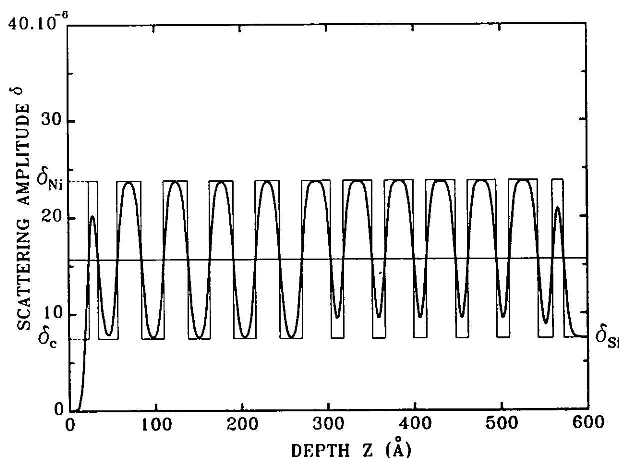

Fig. 6. Index profile corresponding to a fit of the reflectivity of Fig. 7. The steps symbolize the positions of the interfaces.

4. Experimental results

4.1. *Sample description - reflectivity*

By way of example, we have investigated the transmission of an Ni/C multilayer deposited by sputtering on the (100) surface of a silicon single-crystal wafer. The orientation of the surface was checked by recording the 400 Bragg reflection and no appreciable miscut of the surface with respect to these planes was detected. The deposit includes ten pairs of Ni and C layers. It has been characterized by transmission electron microscopy on cross sections obtained by cleavage perpendicular to the surface, and also by X-ray reflectivity (Rieutord, Benattar, Rivoira, Lepetre, Blot & Luzet, 1989). An index profile corresponding to a fit to these data is shown in Fig. 6. The experimental reflectivity is shown in Fig. 7. The critical angle i_{cf} is 0·33° corresponding to the mean index of nickel and carbon. Note that due to the large electron density of nickel, this critical angle is larger than that of silicon ($i_{cSi} \simeq 0{\cdot}2°$). Classical features of thin stratified deposits are also visible on this curve such as Bragg peaks with secondary maxima.

The model reproduces the main features of the experimental data. Some discrepancies still remain on the intensities of secondary maxima probably due to fluctuations on the individual layer thicknesses that have not been included in the model.

4.2. *Diffraction*

The intensity of the 220 reflection has been recorded for incidences ranging from 0 incident angle to 0 take-off angle.

For angles corresponding to both large input and output angles, the diffraction curve is the same as that for bare silicon, *i.e.* it has the standard shape of asymmetric Bragg reflection. Absorption in the film has a weak effect (less than 1% for $i = 17°$, corresponding to the symmetric case).

4.2.1. *Grazing incidence.* For angles smaller than the critical angle i_{cf}, the intensity is very small

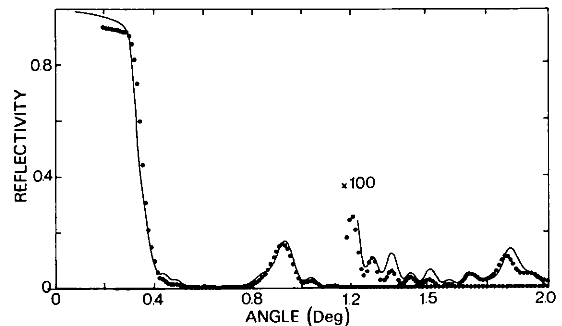

Fig. 7. Reflectivity curve of the multilayer (linear scale). Note the critical angle and the Bragg peak with a secondary maximum on the right.

(Fig. 8). When the incident angle i lies between i_{cSi} and i_{cf}, the incident wave gives rise to an evanescent wave in the film, but which propagates again in the substrate. Thus a small part of the intensity may be allowed to cross the film. However, this zone is hardly seen on the curve because of absorption. Modulations are also visible on the curve, which are due to Kiessig fringes, *i.e.* interferences between the waves reflected at both sides of the film.

At angles greater than i_c, the incident beam can penetrate into the film and the substrate, and the intensity increases rapidly.

At small incidences, the intensity measurements have been performed using rocking curves, *i.e.* φ scans at constant incidence. On each curve we determined the position and the intensity of the maximum. The shift of this position with respect to the geometrical position given by (2) is due to the shift of the Darwin curve with respect to the Bragg position. Its evolution as a function of incidence is shown (Fig. 9). It is in agreement with theoretical calculation but the accuracy of the experimental data is rather poor due to the comparatively large angular dispersion of the incident beam.

In these experiments, we have used a standard copper sealed-tube source. The intensity of the Bragg reflection is close to 10^4 counts s^{-1} at the maximum with our collimation. High counts are required to improve the statistical accuracy and detect small variations in the transmission. Thus, use of synchrotron radiation would allow better accuracy together with an improved collimation of the incident beam.

Another feature characteristic of transmission from multilayers is the hollow peak at $i = 0{\cdot}92°$. This peak corresponds of course to the decrease of intensity in the beam due to the reflection in the Bragg peak of the structure. The relative height and shape of this peak are similar to those of the reflectivity curve of Fig. 7.

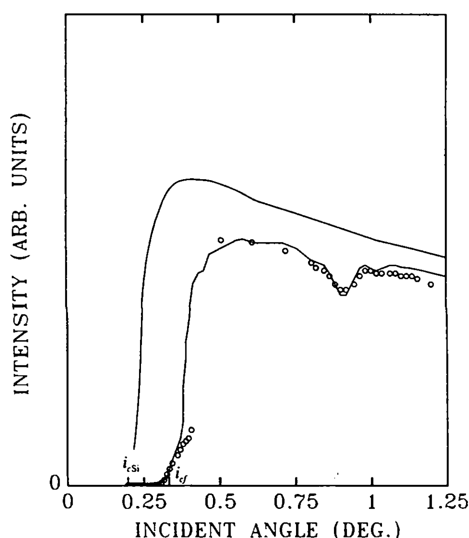

Fig. 8. Small-angle part of the diffracted intensity as a function of incidence. The upper solid line is the calculation for bare silicon and the lower one is for the film using the profile of Fig. 6. Circles are experimental data.

4.2.2. *Grazing-output angle.* On the large angle part of the diffraction curve, similar features are visible (Fig. 10). Now the exit angle is small and decreases with i. A direct comparison with reflectivity is impossible in this case since the corresponding reflectivity (*i.e.* under negative incidence) cannot be measured. The total reflection angle is now related to the difference of indices between the substrate and the film. The measured value $[\theta_c = (i_{ec} - i_S) \cos i_S = 0{\cdot}25°]$ is in good agreement with the theoretical value deduced from the index profile $[(2\delta_F - 2\delta_s)^{1/2} = 0{\cdot}23°]$. The position of the hollow Bragg peak also follows the theoretical prediction of the model. Near i_{ec}, the beam propagating from the substrate to the

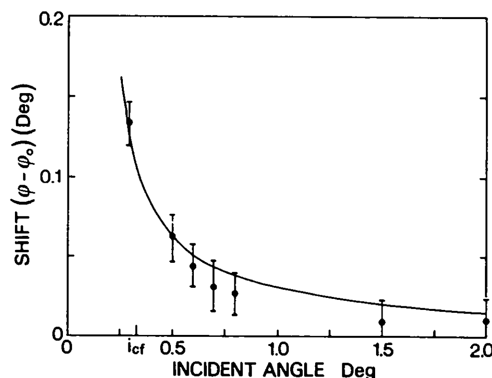

Fig. 9. Shift of the angle φ with respect to its theoretical position φ_0 *versus* incident angle i_0. The solid line represents the theory.

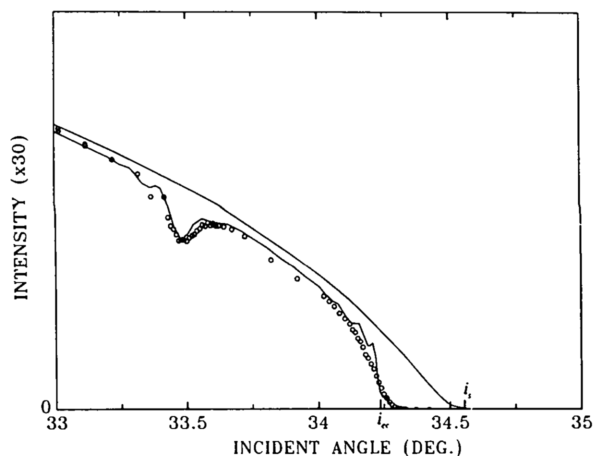

Fig. 10. High-angle part of the diffracted intensity. The angle i_{ec} corresponds to total reflection at the substrate/film interface. i_S is the incidence for zero output angle.

film only partially penetrates the film and probes selectively the region near the interface.

5. Applications

Measuring a transmission coefficient is interesting as a complement to reflectivity. In principle, the information provided by transmissivity T and reflectivity R is the same since for a non-absorbing stratified medium they are related by $R+T=1$. In practice, however: real systems do absorb and their index is not a function of the z coordinate only; and our geometry may allow transmission measurements in cases where reflectivity is not available.

We shall now describe potential applications which stem from these two statements.

5.1. *Rough surfaces*

A very common reason for a system to be not strictly stratified is surface and/or interfacial roughness from lateral height fluctuations, *i.e.* lateral dependence of the electronic density (*i.e.* of the index).

The problem of accounting for roughness in reflectivity calculations has no general solution valid for all kind of roughness. The simplest model consists of an in-plane averaging of the density, modelling the interface by a transition layer in which the index varies smoothly along the normal (Fig. 11).

This approach is justified within the kinematical approximation only, and it may fail in some cases, especially when the penetration length of the radiation is smaller or of the order of the characteristic size of the roughness. This may occur when the penetration length is small (*e.g.* below the critical angle) or when long wavelengths or large amplitudes are present in the roughness.

Roughness has different effects on reflection and transmission (Nevot & Croce, 1980; Nevot, Pardo & Corno, 1988). For instance, the transition-layer model predicts that the reflectivity is damped by a standard Debye–Waller factor $[\exp(-q^2\sigma^2)]$ whereas transmissivity is increased correspondingly, so that all the intensity lost in the reflection arises in the transmission (Pardo, Megademini & Andre, 1988). Obviously, this model cannot account for the scattering by asperities in non-specular directions.

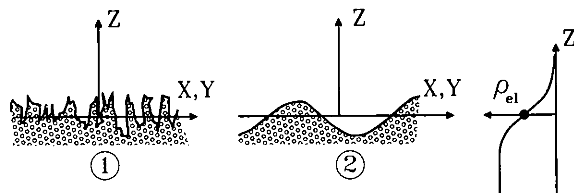

Fig. 11. Two kinds of rough profiles giving the same reflectivity but different transmissivities.

Balancing reflectivity and transmissivity allows a determination of the overall intensity lost in the scattering process and gives information about the spectrum of the roughnesses.

For our systems, no significant discrepancies have been detected between the model and the experiments as the incidence varies. Scattering losses are weak and the transition-layer model applies very well in this case. Systems with greater roughnesses may be better candidates for this kind of study.

5.2. *Buried interfaces*

Another interest of the method is the possibility of achieving grazing incidence for the diffracted beam. This could be used to investigate preferentially the region near the film/substrate interface. Here we have been interested in the transmission information but the same geometry could be adopted for other techniques taking advantage of the shallow penetration of the outgoing beam in the film (such as grazing-incidence fluorescence *etc.*). It should be noted that very few techniques are available for investigations of these kinds of interfaces. Often reflectivity cannot be used since it requires that incident and reflected beams travel over large distances in the substrate.

Concluding remarks

We have demonstrated that transmission measurements in the grazing-incidence mode can be performed to provide information about thin films or surfaces that may complement data from other techniques. From a more general point of view, the technique we describe is another way of taking advantage of the combined substrate/adsorbate scattering to probe the adsorbate. The use of substrate as an 'internal' beam conditioner has been developed in a few other techniques. For instance, we showed in a previous paper (Rieutord, Benattar, Rivoira, Lepetre, Blot & Luzet, 1989) how it could yield the phase of the absorbate structure factor. The standing-wave technique is also based on the use of a substrate-produced standing wavefield to probe the deposit (using fluorescence).

In these techniques combining scattering by perfect crystal and/or grazing incidence, use of dynamical theory is almost compulsory. We have shown that this theory lends itself easily to a combination with other standard thin-film formalisms.

We thank J. J. Benattar for his support and C. Blot for assistance. The experiments were performed at the Service de Physique du Solide et de Résonance Magnétique (SPSRM, CEN Saclay, 91191 Gif-sur-Yvette, France) of the Commissariat à l'Energie Atomique.

References

ABELÈS, F. (1950). *Ann. Phys. (Paris)*, **5**, 596-640.
AUTHIER, A., GRONKOWSKI, J. & MALGRANGE, C. (1989). *Acta Cryst.* **A45**, 432-441.
BATTERMAN, B. W. & COLE, H. (1964). *Rev. Mod. Phys.* **36**, 681-717.
BEDYNSKA, T. (1973). *Phys. Status Solidi A*, **19**, 365-372.
BEDYNSKA, T. (1974). *Phys. Status Solidi A*, **25**, 405-411.
BEDZYK, M. J., BOMMARITO, G. M. & SCHILDKRAUT, J. S. (1989). *Phys. Rev. Lett.* **62**, 1376-1379.
BORN, M. & WOLF, E. (1984). *Principles of Optics*, 6th ed., pp. 51-70. Oxford: Pergamon.
BRÜMMER, O., HÖCHE, H. R. & NIEBER, J. (1976). *Phys. Status Solidi A*, **33**, 587-593.
BRUNEL, M. (1986). *Acta Cryst.* **A42**, 304-309.
BRUNEL, M. & DE BERGEVIN, F. (1986). *Acta Cryst.* **A42**, 299-303.
COWAN, P. L. (1985). *Phys. Rev. B*, **32**, 5437-5439.
DOSCH, H., BATTERMAN, B. W. & WACK, D. C. (1986). *Phys. Rev. Lett.* **56**, 1144-1147.
DURBIN, S. M. & GOG, T. (1989). *Acta Cryst.* **A45**, 132-141.
HARTWIG, J. (1976). *Phys. Status Solidi A*, **37**, 417-425.
HARTWIG, J. (1977). *Phys. Status Solidi A*, **42**, 495-500.
JAMES, R. W. (1982). *The Optical Principles of the Diffraction of X-rays*. Woodbridge, Connecticut: Ox Bow.
KISHINO, S., NODA, A. & KOHRA, K. (1972). *J. Phys. Soc. Jpn*, **33**, 158-166.
MARRA, W. C., EISENBERGER, P. & CHO, A. Y. (1979). *J. Appl. Phys.* **50**, 6927-6933.
NEVOT, L. & CROCE, P. (1980). *Rev. Phys. Appl.* **15**, 761-779.
NEVOT, L., PARDO, B. & CORNO, J. (1988). *Rev. Phys. Appl.* **23**, 1675-1686.
PARDO, B., MEGADEMINI, T. & ANDRE, J. M. (1988). *Rev. Phys. Appl.* **23**, 1579-1597.
PARRATT, L. G. (1954). *Phys. Rev.* pp. 359-369.
RIEUTORD, F., BENATTAR, J. J. & BOSIO, L. (1986). *J. Phys. (Paris)*, **47**, 1249-1256.
RIEUTORD, F., BENATTAR, J. J., RIVOIRA, R., LEPETRE, Y., BLOT, C. & LUZET, D. (1989). *Acta Cryst.* **A45**, 445-453.
RUSTICHELLI, F. (1975). *Philos. Mag.* **31**, 1-12.
SAKATA, O. & HASHIZUME, H. (1988). *Jpn. J. Appl. Phys.* **27**, L1976-L1979.
SAUVAGE, M. (1989). Private communication.
VINEYARD, G. (1982). *Phys. Rev. B*, **26**, 4126-4159.

SHORT COMMUNICATIONS

Contributions intended for publication under this heading should be expressly so marked; they should not exceed about 1000 *words; they should be forwarded in the usual way to the appropriate Co-editor; they will be published as speedily as possible.*

Acta Cryst. (1990). **A46**, 534-536

Comments on papers on quantitative phase determination from three-beam diffraction by Chang and Tang (1988).

By K. HÜMMER and E. WECKERT, *Institut für Angewandte Physik, Lehrstuhl für Kristallographie der Universität, Bismarckstrasse* 10, *D*-8520 *Erlangen, Federal Republic of Germany*

(*Received* 14 *June* 1989; *accepted* 9 *January* 1990

Abstract

In two papers [Chang & Tang (1988). *Acta Cryst.* **A44**, 1065-1072 and Tang & Chang (1988). *Acta Cryst.* **A44**, 1073-1078] the authors are confused with respect to the rotation sense of the crystal lattice during a Renninger ψ-scan experiment. This leads to wrong phase determination. We show that the definition of the triple phase sum involved in a three-beam case used by Chang & Tang is not valid if strong anomalous-dispersion effects must be taken into account.

The asymmetry of the integrated ψ-scan profiles scanning through a three-beam position contain information on the phase difference between the directly diffracted wave (primary reflection) generated by diffraction of the incident beam at the lattice planes of the reciprocal-lattice vector (r.l.v.) **G** and the 'Renninger *Umweg*' wave generated by simultaneous diffraction at the lattice plane of the r.l.v.'s **L** (secondary reflection) and **G** − **L**.*

[Parenthetic note: The schematic representation of the three-beam interaction in Fig. 1.1 of the review article of Chang (1987) is wrong. The diffraction condition of the incident beam with respect to the lattice planes **G** − **L** is not fulfilled. In a three-beam case **0**/**G**/**L**, three strong wave fields are excited with wave vectors **K**(**0**), **K**(**G**) and **K**(**L**). A wave field with **K**(**G** − **L**) does not exist.]

It is well known and proved theoretically and experimentally that the asymmetry of a ψ-scan profile depends also on the rotation sense of the reciprocal lattice relative to the Ewald sphere, independent of the special three-beam position selected from the two possible three-beam positions for each individual three-beam case.

To be clear in the nomenclature for the rotation sense, we define the following: A ψ scan through a three-beam position is called an 'in-out' ψ scan when the second r.l.v. **L** lies inside the Ewald sphere at the beginning of the ψ scan and outside at the end of the ψ scan. In Chang's (1987)* nomenclature, this is called an outgoing position. The opposite rotation sense, an out-in scan, is called by Chang the incoming position.

* Here we use the nomenclature of Chang & Tang (1988) and Tang & Chang (1988).

* For simplicity in citation we refer to the review article of Chang (1987), where the previous papers of Chang *et al.* are summarized.

0108-7673/90/060534-03$03.00 © 1990 International Union of Crystallography